Supplementary Information for

Satellite quantification of oil/gas methane emissions in the US and Canada including contributions from individual basins

Lu Shen*, Ritesh Gautam, Mark Omara, Daniel Zavala-Araiza, Joannes D. Maasakkers, Tia R. Scarpelli, Alba Lorente, David Lyon, Jianxiong Sheng, Daniel Varon, Hannah Nesser, Zhen Qu, Xiao Lu, Melissa P. Sulprizio, Steven P. Hamburg, Daniel J. Jacob

*Corresponding author: Lu Shen (lshen@pku.edu.cn)

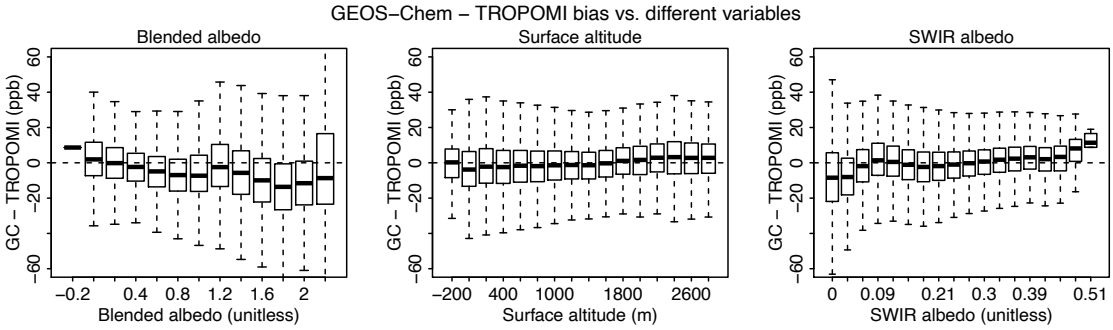

Fig. S1. The relationship of the bias of GEOS-Chem and TROPOMI with (a) blended albedo, (b) surface altitude, and (c) SWIR albedo across the US and Canada from May 2018 to February 2020.

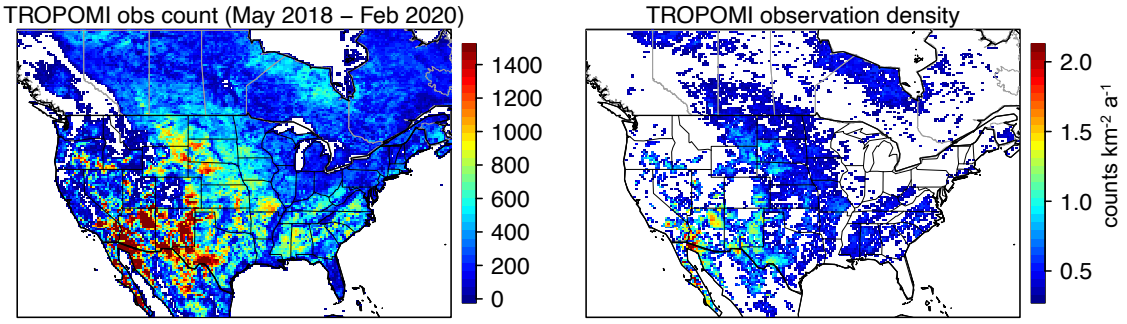

Fig. S2. (a) Number of TROPOMI observations from May 2018 to February 2020, mapped to 0.25°x0.325° horizontal resolution. (b) Same as (a) but for the TROPOMI data density (counts km^{-2} a^{-1}).

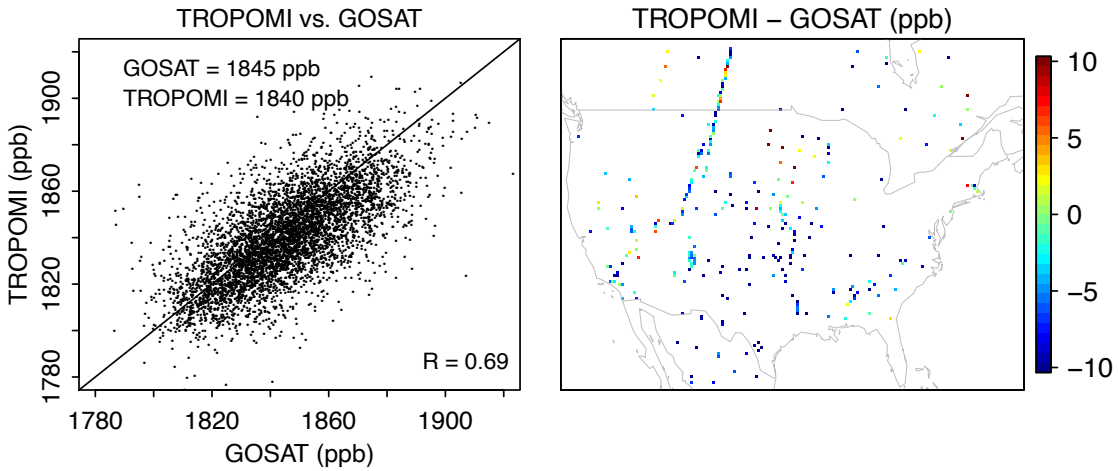

Fig. S3. Comparison between TROPOMI and GOSAT. (a) Scatter plot of all observations in north America from May 2018 to February 2020. Both TROPOMI and GOSAT data are mapped to a 0.3125° x 0.25° horizontal resolution. The mean concentrations from GOSAT and TROPOMI data are shown in the legend (left plot). (b) Spatial distribution of the bias between TROPOMI and GOSAT data.

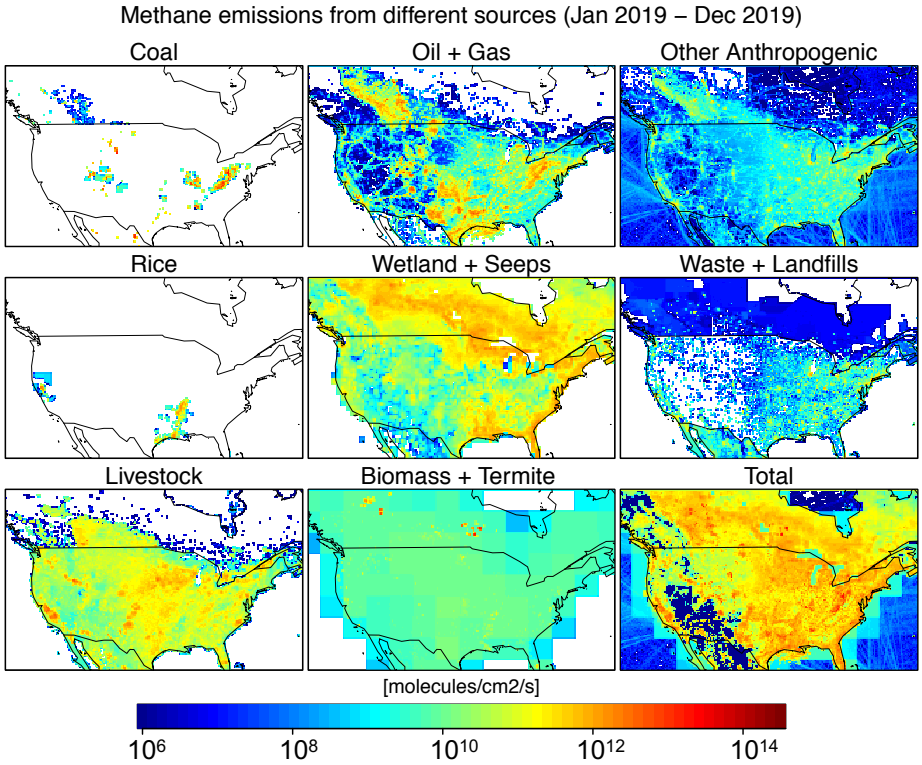

Fig. S4. Prior estimates of methane emissions from different sectors in North America, mapped to the 0.25°x0.3125° resolution. We use the anthropogenic emissions inventory for the US from Maasakkers et al. (2016) for 2012, and the O/G emissions are updated to the year 2018 based on activity data in the Enverus DrillingInfo database (Enverus DrillingInfo, 2020). For Canada, we use anthropogenic emissions from Scarpelli et al. (2021) based on the Environment and Climate Change Canada's (ECCC) inventory for 2018 (ECCC, 2020).

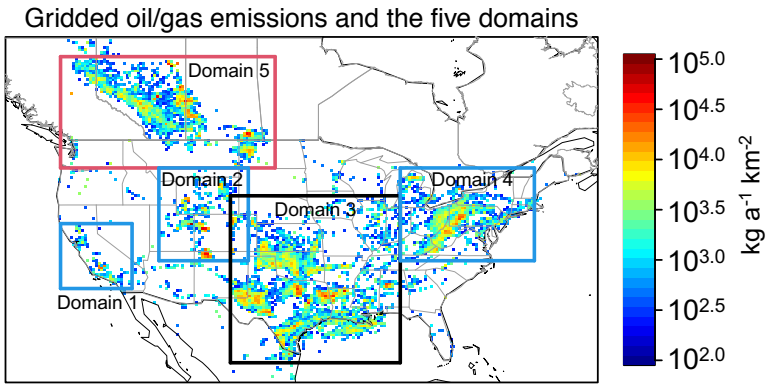

Fig. S5. The five domains used in this study, which can account for 98% O/G emissions in the continental US and Canada.

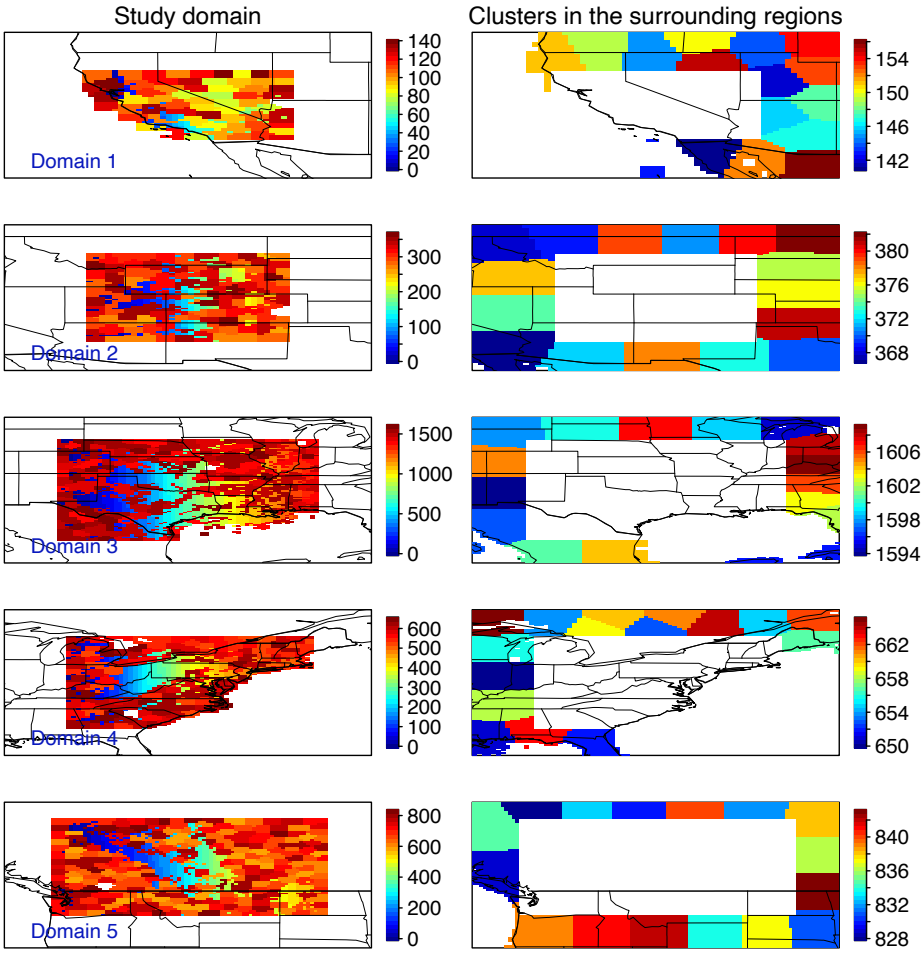

Fig. S6. Native gridcells and clusters in the state vector for each domain. Labels in left column refer to the native gridcells and clusters inside each domain. Labels in right column refer to the clusters outside each domain.

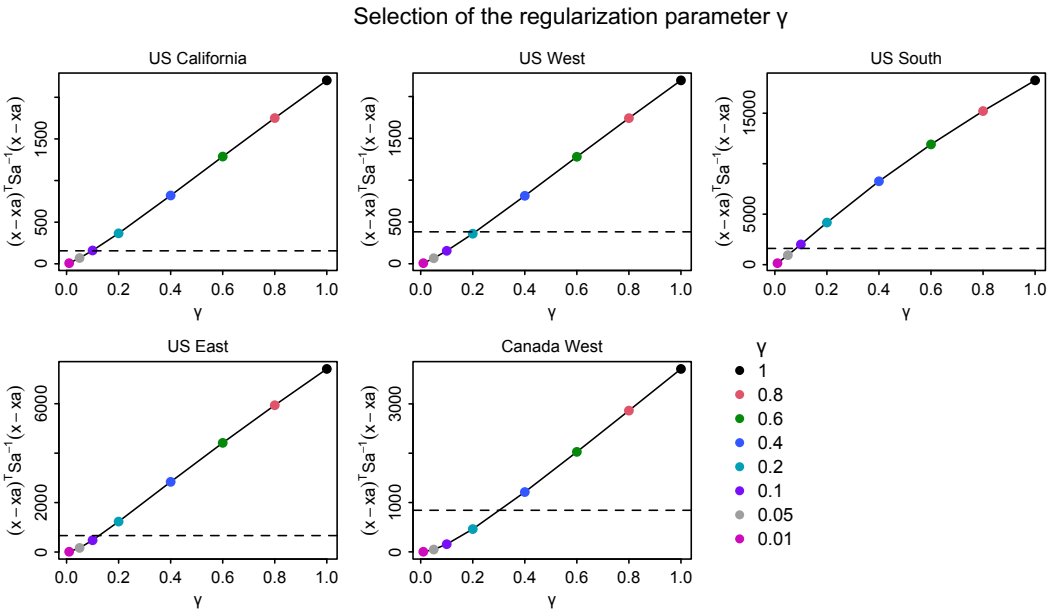

Fig. S7. Squared errors of a regularized solution versus different values of γ. The optimal value of γ can be selected when $(\hat{x} - x_A)^T {S_A}^{-1} (\hat{x} - x_A)) \approx n$, where n is the number of prior terms that can be found in Table S2 and are shown as the dashed line in each plot. We use γ=0.2 in the main text and also test the sensitivity of our results to γ=0.1 and γ=0.4.

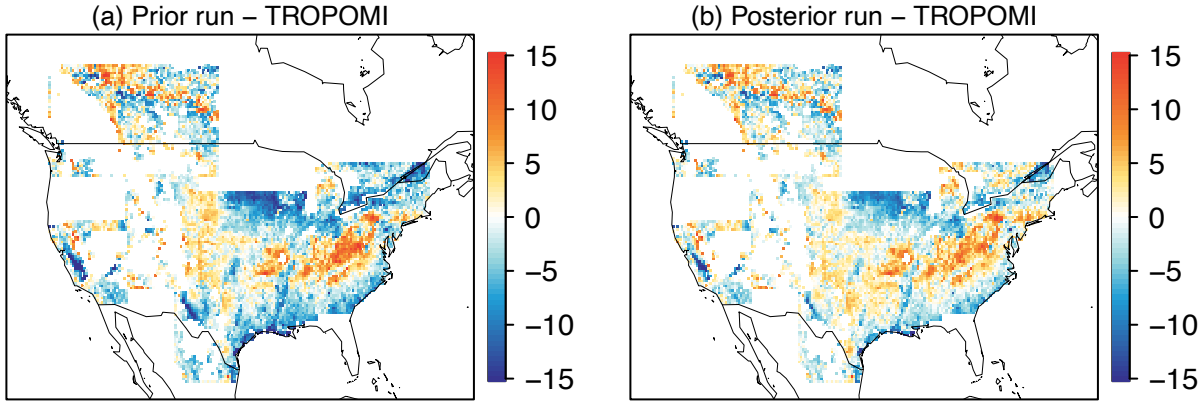

Fig. S8. (a) The bias of column-averaged methane mixing ratio between the forward model using the prior emissions and TROPOMI, as averaged from May 2018 to February 2020. (b) Same as (a) but for the forward model using the posterior estimates. Here we only show the gridboxes where the averaging kernel sensitivity is higher than 0.01 in Fig. S9.

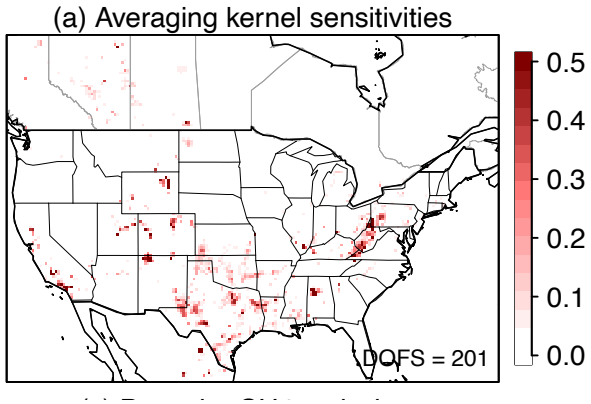

Fig. S9. Averaging kernel sensitivities representing the diagonal terms of the averaging kernel matrix. The total degree of freedoms (DOFS) is shown inset.

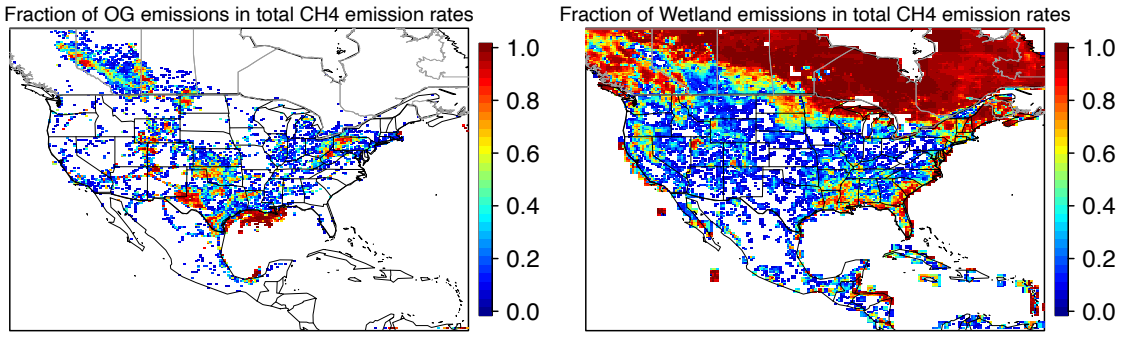

Fig. S10. The fraction of (a) O/G and (b) wetland emission in total methane emission flux (excluding soil absorption here) for each gridcell. See Methods for more details about the emission inventories.

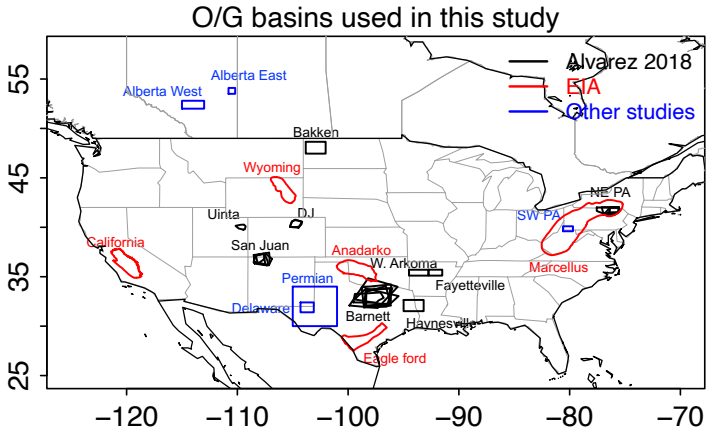

Fig. S11. Map of O/G basins in this study. Black polygons represent estimated boundaries of aircraft sampled source regions (different polygons denote different flight paths), with the shapefiles provided by Alvarez et al. (2018). For these basins with multiple flight paths, we only show the one with the largest size in Figure 1-2. Blue polygons are basin boundaries from other studies, including Johnson et al. (2017) for Alberta East, Zavala-Araiza et al. (2018) for Alberta West, Ren et al. (2019) for SW PA, Zhang et al. (2020) for Permian, and Lyon et al. (2021) for Delaware. Red polygons represent other major O/G basins from US Energy Information Administration (EIA, https://www.eia.gov/maps/maps.htm).

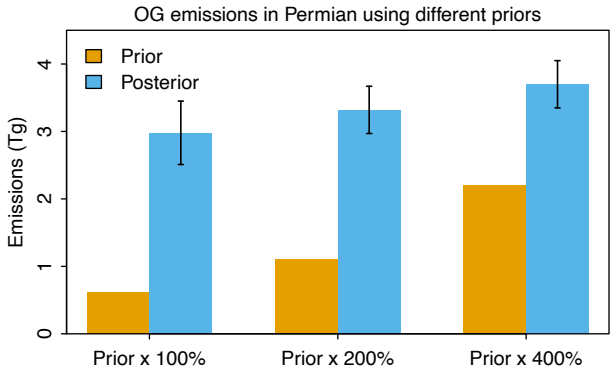

Fig. S12. Posterior emissions in Permian after applying different scaling factors (100%, 200% and 400%) to oil/gas production sector of the priors. The prior O/G emissions are thus 0.62, 1.1 and 2.2 Tg a^{-1} in Permian. Vertical bars indicate the 2x error standard deviations from the inversion ensemble.

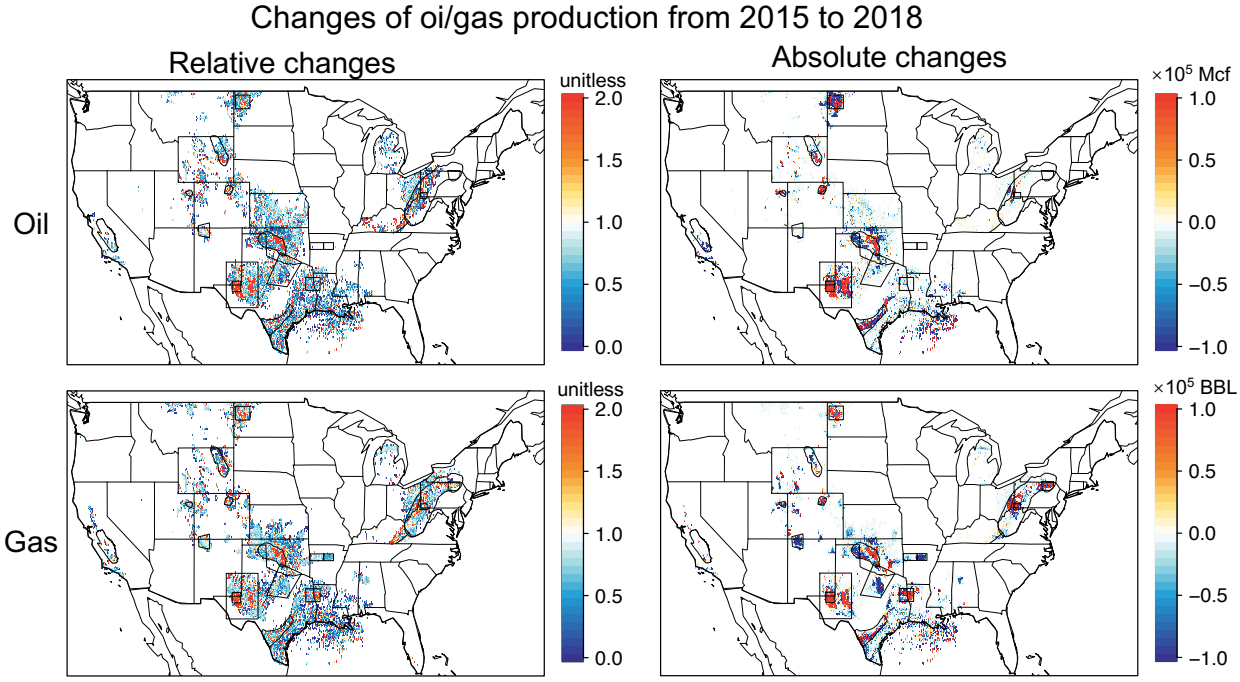

Fig. S13. Relative and absolute changes of oil/gas production from 2015 to 2018 from Enverus Drilling Info (Enverus DrillingInfo, 2020).

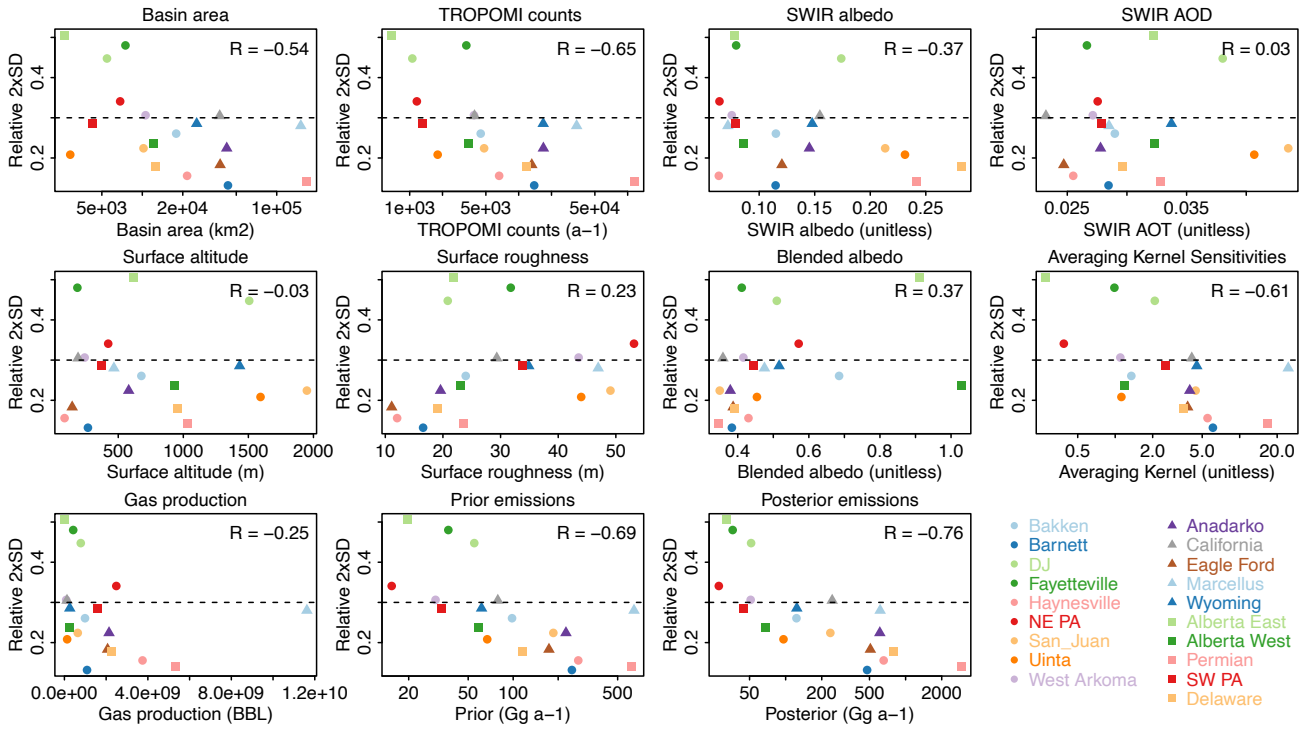

Fig. S14. Same as Fig. 5 but for more variables, including short-wave infrared (SWIR) albedo, SWIR aerosol optical depth, surface altitude, surface roughness (standard deviation of surface altitudes), blended albedo, gas production.

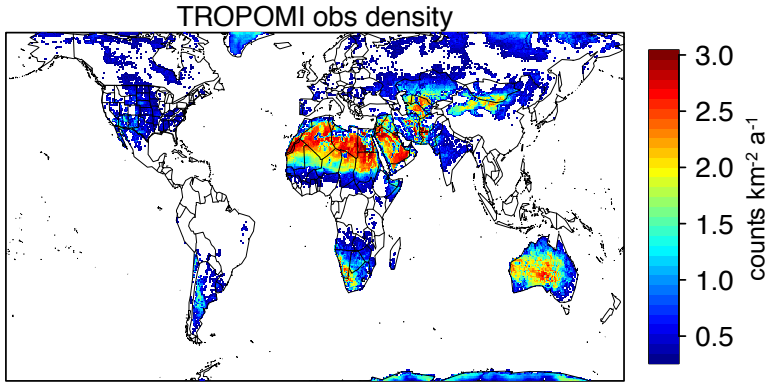

Fig. S15. Same as Fig. S2b, but for TROPOMI data density globally. Gridcells with density < 0.3 counts km^{-2} a^{-1} are shown as white.

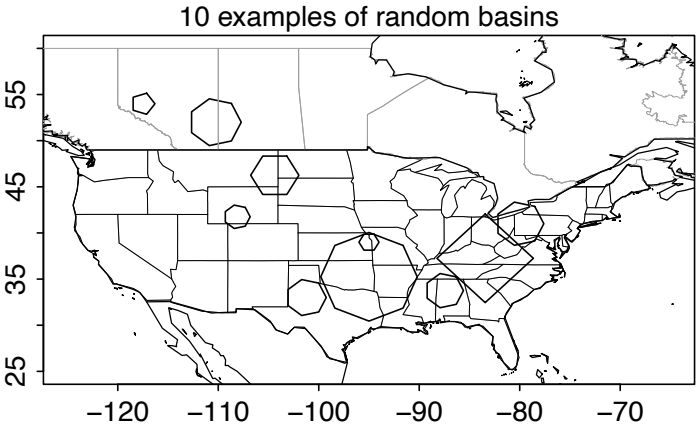

Fig. S16. Ten examples of pseudo O/G basins. We generate 1,000 pseudo O/G basins with varying locations and area sizes across North America and here we show 10 examples of them.

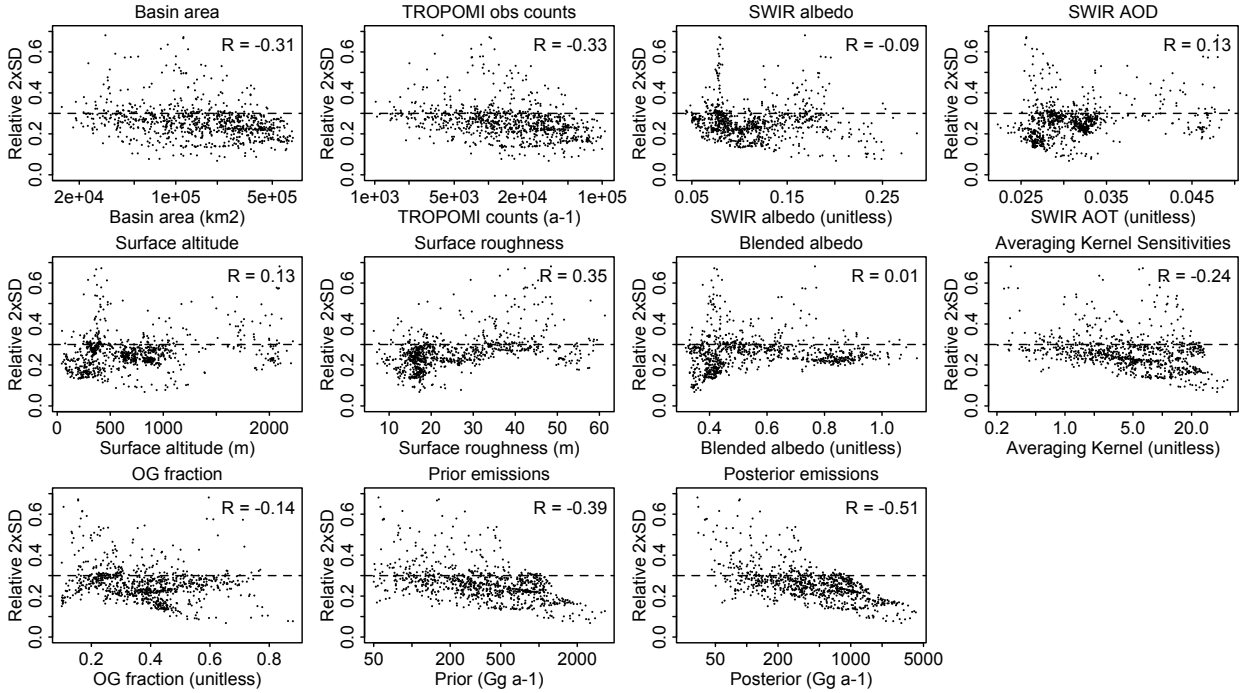

Fig. S17. Same as Fig. S14 but for 1,000 pseudo-basins that are generated randomly with varying locations and area sizes in the study domain. The correlation coefficients are shown inset.

Table S1. Oil and natural gas emission fluxes by field estimates, national bottom-up estimates and TROPOMI top-down inversion in major oil/gas basins in the US and Canada.

Basin names	Reference for the field measurements	Years of field measurements	Field estimates (Gg a^{-1})	Bottom-up estimates by Alvarez et al. (Alvarez et al., 2018) for 2015	Bottom-up estimates by US EPA and ECCC for 2018 (Gg a^{-1})	Top-down estimates by TROPOMI for 2018-202
Bakken	Peischl et al. (2016)	2014	237	210	98	123
Barnett	Karion et al. (2015)	2013	526	499	247	478
DJ	Pétron et al. (2014)	2012	166	184	55	52
Fayetteville	Schwietzke et al. (2017)	2015	272	201	37	36
Haynesville	Peischl et al. (2015)	2013	639	639	273	656
NE PA	Barkley et al.(2017)	2015	131	175	15	28
San Juan	Smith et al. (2017)	2015	499	499	186	236
Uinta	Karion et al. (2013)	2012	482	254	67	96
West Arkoma	Peischl et al. (2015)	2013	228	114	30	51
Alberta East	Johnson et al. (2017)	2016	59		19	32
Alberta West	Zavala-Araiza et al. (2018)	2016	42		59	68
Permian	EDF (2019)	2018	2663		620	2550*
SW PA	Ren et al. (2019)	2015	11		33	64
Delaware	Lyon et al. (2021)	2019-2020	1542		116	800**

* We use the posterior estimates in Permian Basin from May 2018 to March 2019 here to match the sampling period by EDF (2019).

** We use the posterior estimates in Delaware from April 2019 to February 2020 here to match the sampling period by Lyon et al. (2021).

Table S2. Number of native gridcells and clusters in each domain[1] of the US and Canada.

	Native gridcells	Clusters inside each domain	Clusters outside each domain	Length of the state vector
California	77	62	16	155
US Mountain West	264	101	16	381
US South	1368	224	16	1608
US Northeast	516	132	16	664
Canada West	577	249	16	842
Total	2802	768	80	3650

[1]Details of these domains can be found in Fig. S5-S6.

Table S3. TROPOMI retrieval parameters, emissions and oil/gas production in major O/G basins.

	Area (km^2)	Observation counts (a^{-1})	SWIR[1] albedo	Aerosol optical depth	Surface altitude (m)	Surface Roughness[2] (m)	Prior emissions ($Gg\ a^{-1}$)	Posterior emissions ($Gg\ a^{-1}$)	Averaging kernel sensitivity	Relative 2xSD	Oil[3] production(Bbl) in 2019	Gas[3] production (Mcf) in 2019
Bakken	1.8×10^4	5.1×10^3	0.12	0.03	678	24	98	123	1.3	26%	4.5×10^8	9.9×10^8
Barnett	4.3×10^4	1.4×10^4	0.11	0.03	267	17	247	478	6.1	13%	8.1×10^6	1.1×10^9
DJ	5.5×10^3	1.1×10^3	0.17	0.04	1506	21	55	52	2.1	45%	1.3×10^8	7.8×10^8
Fayettevil le	7.5×10^3	3.3×10^3	0.08	0.03	186	32	37	36	1.0	48%	0	4.2×10^8
Haynesvil le	2.2×10^4	6.6×10^3	0.06	0.03	88	12	273	656	5.5	16%	5.9×10^6	3.7×10^9
NE PA	6.8×10^3	1.2×10^3	0.06	0.03	423	53	15	28	0.4	34%	0	2.5×10^9
San Juan	1.0×10^4	4.8×10^3	0.21	0.04	1950	49	186	236	4.4	22%	3.3×10^6	6.4×10^8
Uinta	2.9×10^3	1.8×10^3	0.23	0.04	1593	44	67	96	1.1	21%	7.6×10^6	1.3×10^8
West Arkoma	1.1×10^4	3.9×10^3	0.08	0.03	242	44	30	51	1.1	31%	1.1×10^3	8.6×10^7
Anadarko	4.2×10^4	1.7×10^4	0.15	0.03	580	20	226	610	4.0	22%	1.4×10^8	2.1×10^9
California	3.8×10^4	3.9×10^3	0.15	0.02	191	29	79	244	4.1	30%	1.1×10^8	1.2×10^8
Eagle Ford	3.8×10^4	1.3×10^4	0.12	0.02	146	11	174	508	3.8	18%	4.6×10^8	2.1×10^9
Marcellus	1.5×10^5	3.4×10^4	0.07	0.03	467	47	643	613	24.6	28%	4.6×10^7	1.2×10^{10}
Wyoming	2.5×10^4	1.7×10^4	0.15	0.03	1433	35	61	124	4.5	29%	5.1×10^7	2.6×10^8
Alberta East	2.6×10^3	6.8×10^2	0.08	0.03	619	22	19	32	0.3	51%	1.4×10^7	7.9×10^6
Alberta West	1.2×10^4	3.5×10^3	0.09	0.03	929	23	59	68	1.2	24%	1.4×10^7	2.4×10^8
Permian	1.7×10^5	1.1×10^5	0.24	0.03	1030	24	620	2903	16.8	14%	1.6×10^9	5.3×10^9
SW PA	4.3×10^3	1.3×10^3	0.08	0.03	373	34	33	44	2.5	29%	2.4×10^6	1.6×10^9
Delaware	1.2×10^4	1.2×10^4	0.28	0.03	955	19	116	790	3.5	19%	5.5×10^8	2.3×10^9

[1]The short-wave infrared (SWIR) albedo
[2]Surface roughness is defined as the standard deviation of surface altitudes in each satellite pixel.
[3]Oil and gas production are from Enverus DrillingInfo (2020) .

Reference:

Alvarez, R. A., Zavala-Araiza, D., Lyon, D. R., Allen, D. T., Barkley, Z. R., Brandt, A. R., Davis, K. J., Herndon, S. C., Jacob, D. J., Karion, A., Kort, E. A., Lamb, B. K., Lauvaux, T., Maasakkers, J. D., Marchese, A. J., Omara, M., Pacala, S. W., Peischl, J., Robinson, A. L., Shepson, P. B., Sweeney, C., Townsend-Small, A., Wofsy, S. C., and Hamburg, S. P.: Assessment of methane emissions from the U.S. oil and gas supply chain, Science, eaar7204, https://doi.org/10.1126/science.aar7204, 2018.

Barkley, Z. R., Lauvaux, T., Davis, K. J., Deng, A., Miles, N. L., Richardson, S. J., Cao, Y., Sweeney, C., Karion, A., Smith, M., Kort, E. A., Schwietzke, S., Murphy, T., Cervone, G., Martins, D., and Maasakkers, J. D.: Quantifying methane emissions from natural gas production in north-eastern Pennsylvania, Atmos. Chem. Phys., 17, 13941–13966, https://doi.org/10.5194/acp-17-13941-2017, 2017.

ECCC: National Inventory Report 1990-2018: Greenhouse Gas Sources and Sinks in Canada, Environment and Climate Change Canada (ECCC), Gatineau QC, 2020.

EDF: New Mexico oil & gas data, https://www.edf.org/nm-oil-gas/, 2019.

Enverus DrillingInfo: DI Desktop, didesktop.com., 2020.

Johnson, M. R., Tyner, D. R., Conley, S., Schwietzke, S., and Zavala-Araiza, D.: Comparisons of Airborne Measurements and Inventory Estimates of Methane Emissions in the Alberta Upstream Oil and Gas Sector, Environ. Sci. Technol., 51, 13008–13017, https://doi.org/10.1021/acs.est.7b03525, 2017.

Karion, A., Sweeney, C., Pétron, G., Frost, G., Michael Hardesty, R., Kofler, J., Miller, B. R., Newberger, T., Wolter, S., Banta, R., Brewer, A., Dlugokencky, E., Lang, P., Montzka, S. A., Schnell, R., Tans, P., Trainer, M., Zamora, R., and Conley, S.: Methane emissions estimate from airborne measurements over a western United States natural gas field: CH 4 EMISSIONS OVER A NATURAL GAS FIELD, Geophys. Res. Lett., 40, 4393–4397, https://doi.org/10.1002/grl.50811, 2013.

Karion, A., Sweeney, C., Kort, E. A., Shepson, P. B., Brewer, A., Cambaliza, M., Conley, S. A., Davis, K., Deng, A., Hardesty, M., Herndon, S. C., Lauvaux, T., Lavoie, T., Lyon, D., Newberger, T., Pétron, G., Rella, C., Smith, M., Wolter, S., Yacovitch, T. I., and Tans, P.: Aircraft-Based Estimate of Total Methane Emissions from the Barnett Shale Region, Environ. Sci. Technol., 49, 8124–8131, https://doi.org/10.1021/acs.est.5b00217, 2015.

Lyon, D. R., Hmiel, B., Gautam, R., Omara, M., Roberts, K. A., Barkley, Z. R., Davis, K. J., Miles, N. L., Monteiro, V. C., Richardson, S. J., Conley, S., Smith, M. L., Jacob, D. J., Shen, L., Varon, D. J., Deng, A., Rudelis, X., Sharma, N., Story, K. T., Brandt, A. R., Kang, M., Kort, E. A., Marchese, A. J., and Hamburg, S. P.: Concurrent variation in oil and gas methane emissions and oil price during the COVID-19 pandemic, Atmos. Chem. Phys., 21, 6605–6626, https://doi.org/10.5194/acp-21-6605-2021, 2021.

Maasakkers, J. D., Jacob, D. J., Sulprizio, M. P., Turner, A. J., Weitz, M., Wirth, T., Hight, C., DeFigueiredo, M., Desai, M., Schmeltz, R., Hockstad, L., Bloom, A. A., Bowman, K. W., Jeong, S., and Fischer, M. L.: Gridded National Inventory of U.S. Methane Emissions, Environ. Sci. Technol., 50, 13123–13133, https://doi.org/10.1021/acs.est.6b02878, 2016.

Peischl, J., Ryerson, T. B., Aikin, K. C., Gouw, J. A., Gilman, J. B., Holloway, J. S., Lerner, B. M., Nadkarni, R., Neuman, J. A., Nowak, J. B., Trainer, M., Warneke, C., and Parrish, D. D.: Quantifying atmospheric methane emissions from the Haynesville, Fayetteville, and northeastern Marcellus shale gas production regions, J. Geophys. Res. Atmos., 120, 2119–2139, https://doi.org/10.1002/2014JD022697, 2015.

Peischl, J., Karion, A., Sweeney, C., Kort, E. A., Smith, M. L., Brandt, A. R., Yeskoo, T., Aikin, K. C., Conley, S. A., Gvakharia, A., Trainer, M., Wolter, S., and Ryerson, T. B.: Quantifying atmospheric methane emissions from oil and natural gas production in the Bakken shale region of North Dakota, J. Geophys. Res. Atmos., 121, 6101–6111, https://doi.org/10.1002/2015JD024631, 2016.

Pétron, G., Karion, A., Sweeney, C., Miller, B. R., Montzka, S. A., Frost, G. J., Trainer, M., Tans, P., Andrews, A., Kofler, J., Helmig, D., Guenther, D., Dlugokencky, E., Lang, P., Newberger, T., Wolter, S., Hall, B., Novelli, P., Brewer, A., Conley, S., Hardesty, M., Banta, R., White, A., Noone, D., Wolfe, D., and Schnell, R.: A new look at methane and nonmethane hydrocarbon emissions from oil and natural gas operations in the Colorado Denver-Julesburg Basin, J. Geophys. Res. Atmos., 119, 6836–6852, https://doi.org/10.1002/2013JD021272, 2014.

Ren, X., Hall, D. L., Vinciguerra, T., Benish, S. E., Stratton, P. R., Ahn, D., Hansford, J. R., Cohen, M. D., Sahu, S., He, H., Grimes, C., Fuentes, J. D., Shepson, P. B., Salawitch, R. J., Ehrman, S. H., and Dickerson, R. R.: Methane Emissions from the Marcellus Shale in Southwestern Pennsylvania and Northern West Virginia Based on Airborne Measurements, J. Geophys. Res. Atmos., 124, 1862–1878, https://doi.org/10.1029/2018JD029690, 2019.

Scarpelli, T. R., Jacob, D. J., Moran, M., Reuland, F., and Gordon, D.: A gridded inventory of Canada's anthropogenic methane emissions, 2021.

Schwietzke, S., Pétron, G., Conley, S., Pickering, C., Mielke-Maday, I., Dlugokencky, E. J., Tans, P. P., Vaughn, T., Bell, C., Zimmerle, D., Wolter, S., King, C. W., White, A. B., Coleman, T., Bianco, L., and Schnell, R. C.: Improved Mechanistic Understanding of Natural Gas Methane Emissions from Spatially Resolved Aircraft Measurements, Environ. Sci. Technol., 51, 7286–7294, https://doi.org/10.1021/acs.est.7b01810, 2017.

Smith, M. L., Gvakharia, A., Kort, E. A., Sweeney, C., Conley, S. A., Faloona, I., Newberger, T., Schnell, R., Schwietzke, S., and Wolter, S.: Airborne Quantification of Methane Emissions over the Four Corners Region, Environ. Sci. Technol., 51, 5832–5837, https://doi.org/10.1021/acs.est.6b06107, 2017.

Zavala-Araiza, D., Herndon, S. C., Roscioli, J. R., Yacovitch, T. I., Johnson, M. R., Tyner, D. R., Omara, M., and Knighton, B.: Methane emissions from oil and gas production sites in Alberta, Canada, 6, 27, https://doi.org/10.1525/elementa.284, 2018.

Zhang, Y., Gautam, R., Pandey, S., Omara, M., Maasakkers, J. D., Sadavarte, P., Lyon, D., Nesser, H., Sulprizio, M. P., Varon, D. J., Zhang, R., Houweling, S., Zavala-Araiza, D., Alvarez, R. A., Lorente, A., Hamburg, S. P., Aben, I., and Jacob, D. J.: Quantifying methane emissions from the largest oil-producing basin in the United States from space, Sci. Adv., 6, eaaz5120, https://doi.org/10.1126/sciadv.aaz5120, 2020.